**Defining Mitochondrial Cristae Morphology Changes Induced by Aging in Brown Adipose Tissue**

**Authors**: Amber Crabtree[1*], Kit Neikirk[1*], Andrea G. Marshall[1*], Larry Vang[1], Dominique Stephens[1], Bryanna Shao[1], Edgar Garza Lopez[2], Jacob Lam[2], Ben Rodriguez[2], Margaret Mungai[2], Jade Stanley[1,3], Danielle Dean[1,3], Jennifer A. Gaddy[4,5], Estevão Scudese[6], Mariya Sweetwyne[7], Jamaine Davis[8], Elma Zaganjor[1], Sandra A. Murray[9], Prasanna Katti[10], Steven M. Damo[11,12], Zer Vue[1#], Antentor Hinton, Jr.[1#]

[1] Department of Molecular Physiology and Biophysics, Vanderbilt University, Nashville, TN, 37232, USA.

[2] Department of Internal Medicine, University of Iowa, Iowa City, IA, 52242, USA

[3] Division of Diabetes, Endocrinology, and Metabolism, Department of Medicine, Vanderbilt University Medical Center, TN, 37232, USA.

[4] Department of Medicine, Vanderbilt University Medical Center, Nashville, TN, 37232, USA.

[5] Tennessee Valley Healthcare Systems, U.S. Department of Veterans Affairs, Nashville, TN, 37232, USA.

[6] Laboratory of Biosciences of Human Motricity (LABIMH) of the Federal University of State of Rio de Janeiro (UNIRIO), Rio de Janeiro, Brazil; Sport Sciences and Exercise Laboratory (LaCEE), Catholic University of Petrópolis (UCP), Brazil.

[7] Department of Laboratory Medicine and Pathology, University of Washington, Seattle, WA, 98195, USA.

[8] Department of Biochemistry, Cancer Biology, Neuroscience, Pharmacology, Meharry Medical College, Nashville, TN 37208 USA

[9] Department of Cell Biology, University of Pittsburgh; Pittsburg h, PA, 15261 USA

[10] National Heart, Lung and Blood Institute, National Institutes of Health, 9000 Rockville Pike, Bethesda, MD 20892, USA.

[11] Department of Life and Physical Sciences, Fisk University, Nashville, TN, 37208, USA.

[12] Center for Structural Biology, Vanderbilt University, Nashville, TN, 37232, USA.

[*] Co-First Authors

[#] Co-Senior Authors

Correspondence:

antentor.o.hinton@vanderbilt.edu

## ABSTRACT

Mitochondria are required for energy production and even give brown adipose tissue (BAT) its characteristic color due to their high iron content and abundance The physiological function and bioenergetic capacity of mitochondria are connected to the structure, folding, and organization of its inner-membrane cristae. During the aging process, mitochondrial dysfunction is observed, and the regulatory balance of mitochondrial dynamics is often disrupted, leading to increased mitochondrial fragmentation in aging cells. Therefore, we hypothesized that the morphological changes in BAT mitochondria and cristae observed across aging would reflect alterations to energy dynamics. We developed a quantitative three-dimensional (3D) electron microscopy approach to map cristae network organization in mouse BAT to test this hypothesis. Using this methodology, we investigated the 3D morphology of mitochondrial cristae in adult (3-month) and aged (2-year) murine BAT tissue via serial block face-scanning electron microscopy (SBF-SEM) and3D reconstruction software for manual segmentation, analysis, and quantification. Upon investigation, we found increases in mitochondrial volume, surface area, and complexity and decreased sphericity in aged BAT. Cristae examination revealed decreased cristae volume, perimeter, and complexity, with cristate appearing more heterogeneous. Overall, these data define the nature of the mitochondrial structure in BAT, showing loss of cristae definition across aging, suggesting alterations in functionality and bioactivity.

## INTRODUCTION

Mitochondria are complex cellular organelles that serve various physiological roles, including maintenance of $Ca^{2+}$ homeostasis, initiation of apoptosis, and cellular energy production [1–3]. With such vital cellular roles, mitochondria must be dynamic to meet the fluctuating energy demands of the cell[1,4,8,9]. The ultrastructure and morphology that mitochondria take is tightly associated with their functional capacity [6]. Therefore, it is no surprise that mitochondrial morphology varies considerably between tissue types and the metabolic health of that tissue [4,5]. Specializations within the inner mitochondrial membrane (IMM), known as cristae, substantially increase the surface area for the oxidative phosphorylation machinery to reside, optimizing energetic capacity [6]. Therefore, maintaining

cristae's structural integrity and spatial arrangement is essential for bioenergetic homeostasis and proper cellular energy production [7].

Normal mitochondrial dynamics consist of well-orchestrated, balanced cycles of fusion and fission that allow for content mixing and quality control to maintain a healthy network [9–11]. Previously, mitochondrial dynamics were thought to only occur with changes in the cellular environment which altered the overall mitochondrial shape. However, both fusion and fission require coordination of not only the outer mitochondrial membrane (OMM), but also coordination and reorganization of the cristae [ref]. Although key regulators for cristae morphology have been identified, the dynamics of cristae reorganization in physiology and disease remain understudied [3x ref].

Mitochondrial oxidative stress and dysfunction are often associated with the pathophysiology of diseases and the aging process, which can lead to the accumulation of mtDNA mutations as well as reactive oxygen species generation[15–17]. The ultrastructural changes that occur with the aging process are only now possible to explore with the development of 3D reconstruction techniques. For example, Faitg *et al*. (2021) showed in murine brain that hippocampal somatic, dendritic, and axonal mitochondria had differential baseline phenotypes and responses to aging [18]. In murine heart, 3D reconstruction revealed aged mitochondria arranged in a less ordered way than their younger counterparts [19]. These findings establish the applicability of 3D reconstruction to study mitochondrial phenotypes and cellular organization. Mitochondrial number, form, and function are highly tissue-dependent [5,12,20]. Brown adipose tissue (BAT) is rich in mitochondria, which are integral in thermogenesis [21]. Brown adipocytes produce heat primarily through the uncoupling of the cristae's proton gradient, which is facilitated through uncoupling protein 1 (UCP1) [24, 26]. In both rodent models and humans, a decrease in BAT thermogenic function has been observed with advanced aging and has been associated with the development of metabolic disorders, including obesity and diabetes. Studies suggest that mitochondrial dysfunction through decreased expression of UCP1 The functional age-related decline in BAT has been associated with mitochondrial dysfunction in several studies. In oxidative-stress-induced models of aging, BAT mitochondria are observed to have decreased expression of UCP1, increased autophagy, and decreased mitochondria size [25]. Yet, to our knowledge, no studies have elucidated changes in the 3D morphology of mitochondria and cristae, as well as their 3D spatial distribution in BAT.

In this study, serial block face-scanning electron microscopy (SBF-SEM) and 3D reconstruction software were utilized to examine the 3D architecture of both mitochondria and cristae in BAT from adult and aged mice. Validated methods of quantification were used to develop a quantitative 3D approach to map mitochondrial networks and cristae. Here, we show that mitochondrial 3D volume, perimeter, 3D area, and complexity index all increase with aging in murine BAT. However, mitochondrial sphericity decreased as age increased. Conversely, mitochondrial cristate showed decreases in 3D volume, perimeter, 3D area, and complexity index while sphericity increased with aging in murine BAT.

## METHODS

### Mice Care Procedure

Male C57BL/6J mice were housed at 22□ C with a 12-h light, 12-h dark cycle accompanied by free access to water and standard chow following birth. Mice were cared for as in Lam *et al*□□ with all protocols approved by the University of Iowa Animal Care and Use Committee (IACUC).

**SBF-SEM Sample Preparation**

Interscapular BAT was excised from 3-month and 2-year aged mice and fixed in 2% glutaraldehyde in 0.1M cacodylate buffer and processed using a heavy metal protocol. BAT samples were then immersed in 3% potassium ferrocyanide, followed by 2% osmium tetroxide for 1 hour each at 4□ C following deionized $H_2O$ (DI $H_2O$) washes. Samples were washed again in diH$_2$O and immersed in filtered 0.1% thiocarbohydrazide for 20 minutes, followed by diH$_2$O washing and subsequent immersion in 2% osmium tetroxide for 30 minutes. Samples were incubated overnight in 1% uranyl acetate at 4□ C. The following day, samples were incubated in 0.6% lead aspartate for 30 minutes at 60□ C prior to an ethanol graded series dehydration. BAT tissue samples were then infiltrated with epoxy Taab 812 hard resin prior to immersion in fresh resin and polymerization at 60□ C for 36-48 hours. The resultant resin blocks were sectioned for transmission electron microscopy (TEM) to identify regions of interest. Samples were then trimmed, glued to an SEM stub, and then placed into a FEI/Thermo Scientific Volumescope 2 SEM. Between 300-400 thin serial sections of 0.09 µm per sample block were obtained and collected. The resultant micrograph blocks were then aligned and manually segmented and reconstructed in 3D using Thermo Scientific Amira Software (Waltham, MA, USA) [27,29].

**Mitochondrial and Cristae Ultrastructure Calculations and Measurements**

Following manual segmentation of mitochondria and cristae in the regions of interest (ROIs), label analyses were performed on each segmented structure using Amira [27]. The SBF-SEM data was acquired from at least three independent experiments to perform blinded-3D structural reconstruction from murine BAT. Manual segmentation of sequential orthoslices was then performed to obtain 300-400 slices of which, 50-100 serial sections were chosen for each 3D reconstruction. Serial sections had approximately equal z-direction intervals and werestacked, aligned, and visualized using Amira software to make videos and quantify volumetric structures. The algorithms for measurements were entered manually (all measurements in the main text) for those not already in the system, and a total of 400 mitochondria from two mice were collected for each quantification.

**Structure Quantifications and Statistic Analyses**

All data obtained from label analyses and manual measurements were statistically analyzed by Student's t-test, or the non-parametric equivalent where applicable, using GraphPad Prism (San Diego, California, USA). All data considered are biological replicates and dots represent individual data points unless otherwise noted. In some cases, for presentation, certain outliers may not be displayed, but all outliers are considered for statistical analysis. Graphs are shown as means with black bars representing the standard error of mean. Tukey post hoc tests were used for multiple comparisons, and a minimum threshold of $p < 0.05$ indicated a significant

difference. Higher degrees of statistical significance (i.e., **, ***, ****) were defined as $p < 0.01$, $p < 0.001$, and $p < 0.0001$, respectively.

## RESULTS

### Mitochondrial and Matrix Volumes Significantly Increase with Aging In BAT

BAT biopsies were collected from adult (3-months-old) and aged (2-years-old) mice and imaged using SBF-SEM. With resolutions of 10 µm for the x- and y-planes and 50 µm for the z-plane, SBF-SEM allows for 3D reconstruction of organelles, providing a high spatial resolution that is unattainable using 2D techniques. To quantify mitochondrial changes across aging, we examined approximately 400 mitochondria from two separate regions of interest per age group were selected from the male mice (n=2) (Figure 1A).. Image stacks of ~50 50-µm ortho slices (Figure 1B) were manually traced at transverse intervals (Figure 1C). This enabled the the generation of of 3D reconstructions of each mitochondrion, as depicted in the flowchart of Figure 1 (Figure 1D).

BAT mitochondria are typically abundant, large, and round in young, healthy tissue [22]. Consistent with this, we observed an abundance of mitochondrial that were spherical in structure in the adult (aged 3-months) is believed to be equivalent to approximately 20-years in the human lifespan. In comparison, the 2-year aged samples are believed to be equivalent to approximately 70 years of age in humans.[30]. When comparing the 3-month to 2-year ages, significant increases in perimeter, 3D area (or surface area), and volume were observed (Figure 2). When comparing the mitochondrial quantifications from each mouse, they exhibited minimal inter-group heterogeneity but consistent intra-individual variability with increased heterogeneity in aged samples.

### BAT Aging Significantly Increases Mitochondrial Complexity

Brown adipocytes are an integral part of BAT and are generally classified as either being high-thermogenic or low-thermogenic. High thermogenic brown adipocytes are characterized by both smaller lipid size, round-shaped mitochondria, and a high basal respiration rate [32]. Conversely, low thermogenic brown adipocytes are characterized by larger lipids, oval-shaped mitochondria, and a low basal respiration rate. Interestingly, a reduced thermogenic capacity is associated with aging and obesity [32]. Thus, characterizing the shape of mitochondria may have important implications for their overall functional state.

Viewing the overall complexity of mitochondria can provide relative insights into the complexity of the mitochondrial networks they form as seen in skeletal and cardiac tissue [12]. The sphericity of mitochondria, or the closeness something is in shape to a perfect sphere, shows a significant decrease across aging (Figure 3C). Of note, high-thermogenic BAT mitochondria are round whereas low-thermogenic mitochondria are considered oval in shape. The mitochondrial complexity index (MCI) is an index that correlates with the complexity of the mitochondrial shape, such as surface area and branching relative to volume ($\text{Surface Area}^3 / 16\pi^2 \text{volume}^2$). As an analogous measure for sphericity, it remains consistent for mitochondria with the same shape but different volumes, as demonstrated by 3D model simulations [33]. The MCI showed increases in mitochondrial complexity across aging (Figure 3D). To visualize how

mitochondrial complexity is changed across mitochondrial volume, we performed a technique known as mito-otyping, which organizes mitochondria based on their volume for each aging point (Figure 3E). Importantly, using this technique allows for the simultaneous visualization of changes in the complexity and volume across our aging model at each volume point analyzed.

### Aged BAT Mitochondria Show Altered Cristae Volume, Area, and Perimeter

Mitochondrial morphology is tightly associated with mitochondrial function, making it an important component that is often unexplored. Alterations in cristae morphology and matrix volume can provide equally important quantitative changes in BAT aging. Although there are morphological restraints, increased cristae volume generally correlates with an increased ATP potential [34]. Notably, inflammation of BAT has been demonstrated to cause loss of cristae structural integrity, possibly related to impaired UCP1 activation also observed [35]. Therefore, we sought to quantify cristae morphological and size changes across aging. Using the workflow of SBF-SEM-based 3D reconstruction for BAT cristae, bwas obtained from mice (Figure 4A), and 10 µm by 10 µm orthoslices were overlaid for 3D reconstruction (Figure 4B). Representative orthoslices from the SBF-SEM sectioning were used to generate a detailed 3D reconstruction of cristae (Figure 4C-D).

Cristae and matrix morphology changes across aging indicate that cristae in the 2-year BAT are more heterogenous in size, but are generally smaller and less complex than those in the 3-month samples. Interestingly, while the mitochondrial parameters measured increased overall, we observe the opposite here, where cristae volume, surface area, and perimeter exhibit a significant decrease. Despite increased heterogeneity and larger outliers, this data indicates cristae density is reduced across aging in BAT.

### Aged BAT Mitochondria Show Altered Cristae Complexity

Perturbed cristae morphology has been associated with enlarged and dysfunctional mitochondria [6,36]. Observations of aberrant cristae in senescent cells have also been noted as being partially lost, totally lost, or in circular formation [36]. To understand the morphological changes that occur with cristae across aging, cristae complexity was examined in the 3-month and 2-year aged samples (Figure 6). Notably, these findings resemble those observed for volume, with reduced cristae complexity observed in aged murine BAT. Mito-otyping was utilized to compare cristae morphology in samples from 3-month and 2-year aged groups across volumes (Figure 6E).The 2-year aged sample showed the presence of mitochondria with partially lost cristae, along with circular cristae. Notably, we also observed “island” shaped cristae which were smaller and fragmented. The findings confirm that cristae in 2-year samples are not only more heterogeneous in size but also generally smaller and less complex than those in 3-month samples.

## DISCUSSION

In this study, we examined the mitochondrial ultrastructure changes that occur in murine BAT with aging using SBF-SEM and 3D reconstruction. With the utilization of these tools, increases in mitochondrial 3D volume, perimeter, 3D area, and complexity index as well as decreases in sphericity were quantified between adult and aged murine BAT. Cristae from adult and aged

murine BAT showed decreases in 3D volume, perimeter, 3D area, and complexity index while increased sphericity was observed with aging. (Figures 2, 3, 5). Interestingly, increases in mitochondrial area and perimeter, but not cristae area and perimeter, indicate an increase in mitochondrial matrix volume with aging in murine BAT. (Figure 2D-E). ITheresults presented here also indicate that both mitochondrial and matrix volumes increase with aging, but not cristae volume, in murine BAT. Previous studies have noted the presence of mitochondrial swelling in cases of mitochondrial dysfunction and membrane potential loss [36,39,40]. Under extreme conditions, osmotic swelling of the mitochondrial matrix follows the opening of the inner membrane permeability transition pore (PTP) and can also irreversibly engage in apoptosis [42–44]. Notably, the intermembrane proteins released include cytochrome C and apoptosis-inducing factor (AIF) which solidify the apoptotic pathway [42–44].

Another interesting observation in our study is the presence of circular cristae in the aged BAT samples that were not present in the young BAT samples. Circular cristae have been described in senescent cells by others and differ from onion cristae [47] given the lack of multiple rings of cristae present [36]. The presence of circular cristae have also been noted in senescent cells [36], but a lack of 3D studies of cristae morphology makes it difficult to make comparisons in cristae phenotypes. Beyond this, it is evident that the aging process decreases overall mitochondrial cristae density, although the underlying molecular causes have yet to be elucidated (Figure 5C).

Although the findings here show clear mitochondrial and cristae alterations with aging, it should be noted that murine and human BAT have several key differences. Future studies are needed to understand morphological changes of mitochondria and cristae in human BAT in comparison to murine BAT. Studies have shown that while cristae architecture remains pertinent for energetic capacity across models, aging shows differed functional and structural changes in mice and *Drosophila* [65]. An important limitation of our study that should be noted is that other studies have shown distinct populations of adipocytes, with higher-thermogenic activity populations, which can dynamically form in exposure to cold [67]. Our study did not account for this heterogeneity in the population, which may account for some of the variation observed in mitochondrial structure. Future studies may consider 3D tissue profiling to see if mitochondrial and cristae structure varies across populations of adipocytes or alterations in gene expression [67].

In conclusion, to our knowledge, we are the first to elucidate the alterations in 3D mitochondrial and cristae structures across the murine aging process in BAT. Of relevance, this aids to establish standards for the phenotypes presented. Importantly, the phenotypes found here may be related to pre-stress states, alterations in membrane potential, changes in fusion or cristae proteins, sex-dependent differences, or changes in metabolic pathways. Although this study did not delve into the molecular changes that influence the aging phenotypes observed, by establishing these 3D structures, future studies investigating the influence of aging in BAT on all previously mentioned factors can better understand how these factors may relate to specific phenotypes. In the future, this may aid in establishing standards regarding mitochondrial and cristae structures, to aid future research aimed at developing interventions to mitigate dysfunction during aging in BAT.

## Declaration of interests

The authors have no Conflicts of Interest to declare.

**Acknowledgments**

Funding by the UNCF/Bristol-Myers Squibb E.E. Just Faculty Fund, BWF Career Awards at the Scientific Interface Award, BWF Ad-hoc Award, NIH Small Research Pilot Subaward to 5R25HL106365-12 from the National Institutes of Health PRIDE Program, DK020593, Vanderbilt Diabetes and Research Training Center for DRTC Alzheimer's Disease Pilot & Feasibility Program. T-32, number DK007563 entitled Multidisciplinary Training in Molecular Endocrinology to A.C.; T-32, number DK007563 entitled Multidisciplinary Training in Molecular Endocrinology to Z.V. CZI Science Diversity Leadership grant number 2022- 253529 from the Chan Zuckerberg Initiative DAF, an advised fund of Silicon Valley Community Foundation (to AHJ). NSF EES2112556, NSF EES1817282, NSF MCB1955975, and CZI Science Diversity Leadership grant number 2022-253614 from the Chan Zuckerberg Initiative DAF, an advised fund of Silicon Valley Community Foundation (to S.D.). NSF grant MCB #2011577I and NIH T32 5T32GM133353 to S.A.M.

Figure 1 is arranged using BioRender and all representative images are original.

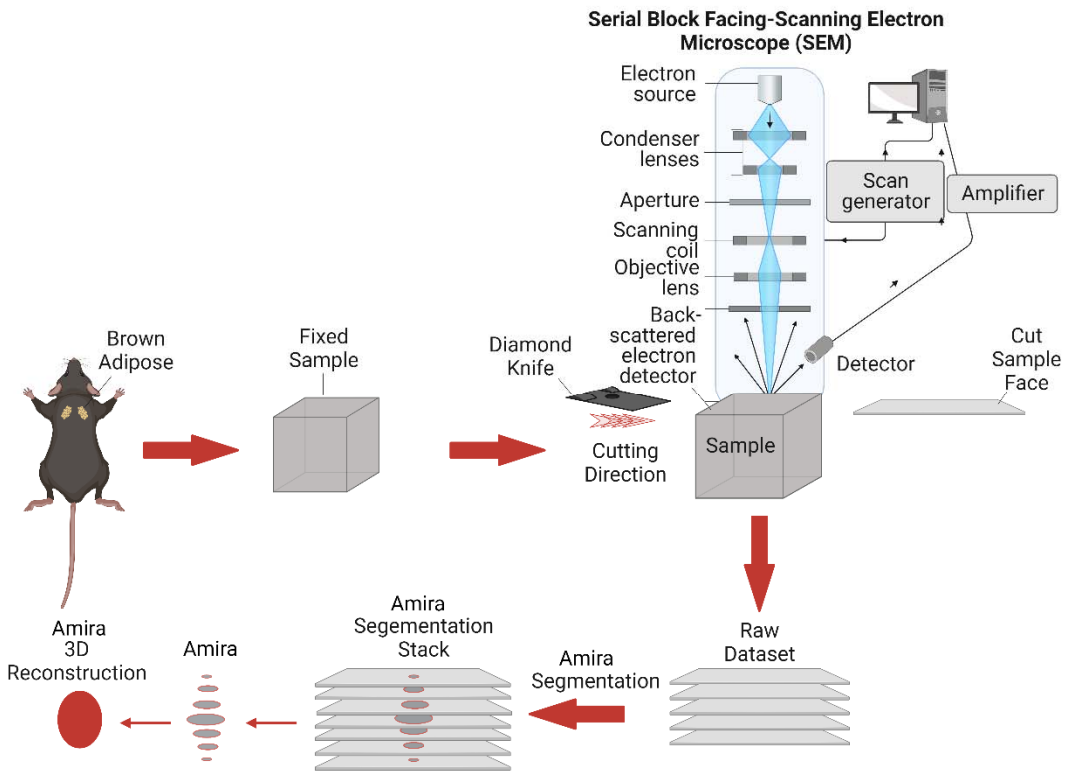


**Figure Legends:**

**Graphical Abstract:** Workflow overview of serial block facing-scanning electron microscopy (SBF-SEM), data segmentation, and 3D analysis of mitochondria using Amira software in murine BAT.

**Figure 1: Detailed 3D reconstruction workflow for mitochondria using serial block face-scanning electron microscopy (SBF-SEM).** (A) Murine brown adipose tissue (BAT) was carefully extracted from skeletal muscle tissue samples. (B) High-resolution 10 µm by 10 µm orthoslices were generated by imaging consecutive ultrathin sections of the sample. These orthoslices were then accurately aligned and stacked to produce a comprehensive 3D volume of the tissue. (C) SBF-SEM images were processed to create representative orthoslices, which provided valuable information on the internal structure of the mitochondria. (D) A detailed 3D reconstruction of the mitochondria was produced based on the orthoslices, allowing for in-depth analysis of mitochondrial morphology and spatial organization.

**Figure 2: Comprehensive analysis of mitochondrial morphology changes during the aging process.** (A) In 3-month-old murine BAT: a representative orthoslice showcases the intricate internal mitochondrial structure, (A') a 3D reconstruction of mitochondria overlaid on the orthoslice illustrates the spatial distribution of mitochondria within the tissue, (A'') and an isolated 3D reconstruction highlights the individual mitochondrial structure. (B) In 2-year-old murine BAT: a representative orthoslice depicts the aged mitochondrial structure, (B') a 3D reconstruction of mitochondria overlaid on the orthoslice demonstrates the spatial organization of aged mitochondria, (B'') and an isolated 3D reconstruction reveals the individual aged mitochondrial structure. (C) Quantitative comparison of 3D mitochondrial volume, (D) surface area, and (E) perimeter between 3-month and 2-year samples to assess morphological differences, revealing age-related changes in size and shape of the mitochondria.

**Figure 3: In-depth analysis of age-related changes in mitochondrial complexity.** (A) In 3-month-old murine BAT: a 3D reconstruction of mitochondria overlaid on the orthoslice offers a comprehensive view of the mitochondrial network, and (A') a transverse perspective of the 3D reconstruction reveals additional details about the spatial organization of the mitochondria. (B) In 2-year-old murine BAT: a 3D reconstruction of mitochondria overlaid on the orthoslice presents an overview of the aged mitochondrial network, and (B') a transverse perspective of the 3D reconstruction displays the spatial organization of the aged mitochondria. (C) Quantitative comparison of 3D sphericity, (D) complexity index, and (E) mito-otyping for mitochondrial morphology in 3-month and 2-year samples based on volume, providing insights into the age-related alterations in mitochondrial organization, shape, and structural complexity.

**Figure 4: Workflow of serial block face-scanning electron microscopy-based 3D reconstruction for cristae. (**A**)** Brown adipose tissue was obtained from 3-month and 2-year mice. (B) 10 µm by 10 µm orthoslices were overlaid for 3D reconstruction. (C) Representative orthoslices from SBF-SEM slices to make (D) cristae 3D reconstruction.

**Figure 5: Cristae Morphology Change across Aging.** (A) In 3-month murine BAT, representative orthoslice (A') 3D reconstruction of mitochondria matrix and cristae overlaid on orthoslice, and (A'') 3D reconstruction isolated mitochondria matrix and cristae (A''') 3D reconstructions of cristae alone (B) In 2-year murine BAT, representative orthoslice (B') 3D reconstruction of mitochondria overlaid on orthoslice, and (B'') 3D reconstruction isolated mitochondria matrix and cristae (B''') 3D reconstructions of cristae alone. (C) Comparisons of cristae 3D volume, (D) 3D area, and (E) 3D perimeter compared in 3-month and 2-year samples.

**Figure 6: Cristae Complexity Change across Aging.** (A) In 3-month murine BAT, 3D reconstruction of cristae viewed from the z-axis, and (A') 3D reconstruction viewed from a transverse point of view (B) In 2-year murine BAT, 3D reconstruction of cristae viewed from the z-axis, and (B') 3D reconstruction viewed from a transverse point of view (C) Comparisons of cristae 3D sphericity, (D) and complexity index in 3-month and 2-year samples. (E) Mito-otyping to compare cristae morphology in samples from 3-month and 2-year across volumes.

**References:**


[1] M. Picard, T. Taivassalo, G. Gouspillou, R. T. Hepple, *The Journal of physiology* **2011**, *589*, 4413.
[2] H. M. McBride, M. Neuspiel, S. Wasiak, *Current Biology* **2006**, *16*, R551.
[3] G. E. Palade, *Anat Rec* **1952**, *114*, 427.
[4] B. Glancy, *Trends in molecular medicine* **2020**, *26*, 58.
[5] M. Picard, D. C. Wallace, Y. Burelle, *Mitochondrion* **2016**, *30*, 105.
[6] S. Cogliati, J. A. Enriquez, L. Scorrano, *Trends in biochemical sciences* **2016**, *41*, 261.
[7] N. Ikon, R. O. Ryan, *Biochimica et Biophysica Acta (BBA) - Biomembranes* **2017**, *1859*, 1156.
[8] A. Y. Seo, A.-M. Joseph, D. Dutta, J. C. Y. Hwang, J. P. Aris, C. Leeuwenburgh, *Journal of Cell Science* **2010**, *123*, 2533.
[9] D. C. Chan, *Annual review of genetics* **2012**, *46*, 265.
[10] F. Dong, M. Zhu, F. Zheng, C. Fu, *FEBS J* **2022**, *289*, 262.
[11] R. J. Youle, A. M. Van Der Bliek, *Science* **2012**, *337*, 1062.
[12] B. Glancy, Y. Kim, P. Katti, T. B. Willingham, *Frontiers in Physiology* **2020**, *11*.
[13] E. Palma, X. Ma, A. Riva, V. Iansante, A. Dhawan, S. Wang, H.-M. Ni, H. Sesaki, R. Williams, W.-X. Ding, S. Chokshi, *Am J Pathol* **2019**, *189*, 580.
[14] Q. Long, D. Zhao, W. Fan, L. Yang, Y. Zhou, J. Qi, X. Wang, X. Liu, *Biophysical journal* **2015**, *109*, 892.
[15] A. Bratic, N.-G. Larsson, *The Journal of clinical investigation* **2013**, *123*, 951.
[16] J. M. Son, C. Lee, *Seminars in Cell & Developmental Biology* **2021**, *116*, 160.
[17] D. A. Chistiakov, I. A. Sobenin, V. V. Revin, A. N. Orekhov, Y. V. Bobryshev, *BioMed Research International* **2014**, *2014*, e238463.
[18] J. Faitg, C. Lacefield, T. Davey, K. White, R. Laws, S. Kosmidis, A. K. Reeve, E. R. Kandel, A. E. Vincent, M. Picard, *Cell Reports* **2021**, *36*, 109509.
[19] J. Messerer, C. Wrede, J. Schipke, C. Brandenberger, M. Abdellatif, T. Eisenberg, F. Madeo, S. Sedej, C. Mühlfeld, *Journal of Anatomy* **2023**, *242*, 91.
[20] E. Herbers, N. J. Kekäläinen, A. Hangas, J. L. Pohjoismäki, S. Goffart, *Mitochondrion* **2019**, *44*, 85.
[21] A. C. Carpentier, D. P. Blondin, F. Haman, D. Richard, *Endocrine Reviews* **2023**, *44*, 143.
[22] G. Frühbeck, S. Becerril, N. Sáinz, P. Garrastachu, M. J. García-Velloso, *Trends in Pharmacological Sciences* **2009**, *30*, 387.
[23] J. Nowack, S. Giroud, W. Arnold, T. Ruf, *Frontiers in Physiology* **2017**, *8*.
[24] A. Graja, S. Gohlke, T. J. Schulz, In *Brown Adipose Tissue* (Eds.: Pfeifer, A.; Klingenspor, M.; Herzig, S.), Springer International Publishing, Cham, **2019**, pp. 55–72.
[25] A. P. A. Macêdo, A. S. R. da Silva, V. R. Muñoz, E. R. Ropelle, J. R. Pauli, *Mechanisms of Ageing and Development* **2021**, *200*, 111598.

[26] J. Darcy, Y.-H. Tseng, *GeroScience* **2019**, *41*, 285.
[27] E. Garza-Lopez, Z. Vue, P. Katti, K. Neikirk, M. Biete, J. Lam, H. K. Beasley, A. G. Marshall, T. A. Rodman, T. A. Christensen, J. L. Salisbury, L. Vang, M. Mungai, S. AshShareef, S. A. Murray, J. Shao, J. Streeter, B. Glancy, R. O. Pereira, E. D. Abel, A. Hinton, *Cells* **2022**, *11*, 65.
[28] J. Lam, P. Katti, M. Biete, M. Mungai, S. AshShareef, K. Neikirk, E. Garza Lopez, Z. Vue, T. A. Christensen, H. K. Beasley, T. A. Rodman, S. A. Murray, J. L. Salisbury, B. Glancy, J. Shao, R. O. Pereira, E. D. Abel, A. Hinton, *Cells* **2021**, *10*, 2177.
[29] K. Neikirk, Z. Vue, P. Katti, B. I. Rodriguez, S. Omer, J. Shao, T. Christensen, E. Garza Lopez, A. Marshall, C. B. Palavicino-Maggio, J. Ponce, A. F. Alghanem, L. Vang, T. Barongan, H. K. Beasley, T. Rodman, D. Stephens, M. Mungai, M. Correia, V. Exil, S. Damo, S. A. Murray, A. Crabtree, B. Glancy, R. O. Pereira, E. D. Abel, A. O. Hinton Jr., *Advanced Biology* **2023**, *n/a*, e2200221.
[30] S. Dutta, P. Sengupta, *Life Sci* **2016**, *152*, 244.
[31] S. Demine, P. Renard, T. Arnould, *Cells* **2019**, *8*, 795.
[32] A. B. Shinde, A. Song, Q. A. Wang, *Front Endocrinol (Lausanne)* **2021**, *12*, 651763.
[33] A. E. Vincent, K. White, T. Davey, J. Philips, R. T. Ogden, C. Lawless, C. Warren, M. G. Hall, Y. S. Ng, G. Falkous, *Cell reports* **2019**, *26*, 996.
[34] K. B. Heine, H. A. Parry, W. R. Hood, *American Journal of Physiology-Regulatory, Integrative and Comparative Physiology* **2023**, *324*, R242.
[35] J. C. de-Lima-Júnior, G. F. Souza, A. Moura-Assis, R. S. Gaspar, J. M. Gaspar, A. L. Rocha, D. L. Ferrucci, T. I. Lima, S. C. Victório, I. L. P. Bonfante, C. R. Cavaglieri, J. C. Pareja, S. Q. Brunetto, C. D. Ramos, B. Geloneze, M. A. Mori, L. R. Silveira, G. R. S. Segundo, E. R. Ropelle, L. A. Velloso, *EBioMedicine* **2019**, *39*, 436.
[36] P. V. S. Vasileiou, K. Evangelou, K. Vlasis, G. Fildisis, M. I. Panayiotidis, E. Chronopoulos, P.-G. Passias, M. Kouloukoussa, V. G. Gorgoulis, S. Havaki, *Cells* **2019**, *8*, 686.
[37] X. Liu, G. Hajnóczky, *Cell Death Differ* **2011**, *18*, 1561.
[38] A. A. Gerencser, J. Doczi, B. Töröcsik, E. Bossy-Wetzel, V. Adam-Vizi, *Biophys J* **2008**, *95*, 2583.
[39] D. Safiulina, V. Veksler, A. Zharkovsky, A. Kaasik, *Journal of Cellular Physiology* **2006**, *206*, 347.
[40] Y. Miyazono, S. Hirashima, N. Ishihara, J. Kusukawa, K.-I. Nakamura, K. Ohta, *Sci Rep* **2018**, *8*, 350.
[41] T. Ahmad, K. Aggarwal, B. Pattnaik, S. Mukherjee, T. Sethi, B. Tiwari, M. Kumar, A. Micheal, U. Mabalirajan, B. Ghosh, S. Roy, A. Agrawal, *Cell death & disease* **2013**, *4*, e461.
[42] J. E. Chipuk, L. Bouchier-Hayes, D. R. Green, *Cell Death Differ* **2006**, *13*, 1396.
[43] V. Gogvadze, S. Orrenius, B. Zhivotovsky, *Biochim Biophys Acta* **2006**, *1757*, 639.
[44] P. X. Petit, M. Goubern, P. Diolez, S. A. Susin, N. Zamzami, G. Kroemer, *FEBS Lett* **1998**, *426*, 111.
[45] B. Niemann, S. Haufs-Brusberg, L. Puetz, M. Feickert, M. Y. Jaeckstein, A. Hoffmann, J. Zurkovic, M. Heine, E.-M. Trautmann, C. E. Müller, A. Tönjes, C. Schlein, A. Jafari, H. K. Eltzschig, T. Gnad, M. Blüher, N. Krahmer, P. Kovacs, J. Heeren, A. Pfeifer, *Nature* **2022**, *609*, 361.
[46] J. Lloberas, J. P. Muñoz, M. I. Hernández-Álvarez, P.-J. Cardona, A. Zorzano, A. Celada, *Autophagy* **2020**, *16*, 2307.
[47] T. Pánek, M. Eliáš, M. Vancová, J. Lukeš, H. Hashimi, *Current Biology* **2020**, *30*, R575.

[48] A. Thirupathi, B. L. da Silva Pieri, J. A. M. P. Queiroz, M. S. Rodrigues, G. de Bem Silveira, D. R. de Souza, T. F. Luciano, P. C. L. Silveira, C. T. De Souza, *J Physiol Biochem* **2019**, *75*, 101.
[49] A. M. Cypess, C. R. Haft, M. R. Laughlin, H. H. Hu, *Cell Metabolism* **2014**, *20*, 408.
[50] G. da N. Silva, A. A. Amato, *Front Cell Dev Biol* **2022**, *10*, 955612.
[51] V. Kozjak-Pavlovic, *Cell and tissue research* **2017**, *367*, 83.
[52] P. Latorre-Muro, K. E. O'Malley, C. F. Bennett, E. A. Perry, E. Balsa, C. D. J. Tavares, M. Jedrychowski, S. P. Gygi, P. Puigserver, *Cell Metabolism* **2021**, *33*, 598.
[53] R. O. Pereira, A. Marti, A. C. Olvera, S. M. Tadinada, S. H. Bjorkman, E. T. Weatherford, D. A. Morgan, M. Westphal, P. H. Patel, A. K. Kirby, *Elife* **2021**, *10*, e66519.
[54] C. Hu, L. Shu, X. Huang, J. Yu, L. Gong, M. Yang, Z. Wu, Z. Gao, Y. Zhao, L. Chen, *Cell death & disease* **2020**, *11*, 1.
[55] A. del Campo, I. Contreras-Hernández, M. Castro-Sepúlveda, C. A. Campos, R. Figueroa, M. F. Tevy, V. Eisner, M. Casas, E. Jaimovich, *Aging* **2018**, *10*, 34.
[56] C. Mancini, S. Gohlke, F. Garcia-Carrizo, V. Zagoriy, H. Stephanowitz, T. J. Schulz, *Sci Rep* **2021**, *11*, 19928.
[57] H. De Vitto, D. B. Arachchige, B. C. Richardson, J. B. French, *Cells* **2021**, *10*, 2603.
[58] E. Zoico, S. Rubele, A. De Caro, N. Nori, G. Mazzali, F. Fantin, A. Rossi, M. Zamboni, *Frontiers in Endocrinology* **2019**, *10*.
[59] I. Lejri, A. Grimm, A. Eckert, *Frontiers in Aging Neuroscience* **2018**, *10*.
[60] Y. Hara, F. Yuk, R. Puri, W. G. M. Janssen, P. R. Rapp, J. H. Morrison, *Proceedings of the National Academy of Sciences* **2014**, *111*, 486.
[61] L. R. Rodríguez, T. Lapeña-Luzón, N. Benetó, V. Beltran-Beltran, F. V. Pallardó, P. Gonzalez-Cabo, J. A. Navarro, *Antioxidants* **2022**, *11*, 165.
[62] C. Pfannenberg, M. K. Werner, S. Ripkens, I. Stef, A. Deckert, M. Schmadl, M. Reimold, H.-U. Häring, C. D. Claussen, N. Stefan, *Diabetes* **2010**, *59*, 1789.
[63] M. P. Mattson, *Ageing Research Reviews* **2010**, *9*, 69.
[64] M. Balcázar, S. Cañizares, T. Borja, P. Pontón, S. Bisiou, E. Carabasse, A. Bacilieri, C. Canavese, R. F. Diaz, F. Cabrera, A. Caicedo, *Front Bioeng Biotechnol* **2020**, *8*, 919.
[65] P. D. Brandt, S. Sturzenegger Varvayanis, T. Baas, A. F. Bolgioni, J. Alder, K. A. Petrie, I. Dominguez, A. M. Brown, C. A. Stayart, H. Singh, *PLoS biology* **2021**, *19*, e3000956.
[66] I. Samuelson, A. Vidal-Puig, *Frontiers in Endocrinology* **2020**, *11*.
[67] A. Song, W. Dai, M. J. Jang, L. Medrano, Z. Li, H. Zhao, M. Shao, J. Tan, A. Li, T. Ning, M. M. Miller, B. Armstrong, J. M. Huss, Y. Zhu, Y. Liu, V. Gradinaru, X. Wu, L. Jiang, P. E. Scherer, Q. A. Wang, *J Clin Invest* **2020**, *130*, 247.

# Graphical Abstract

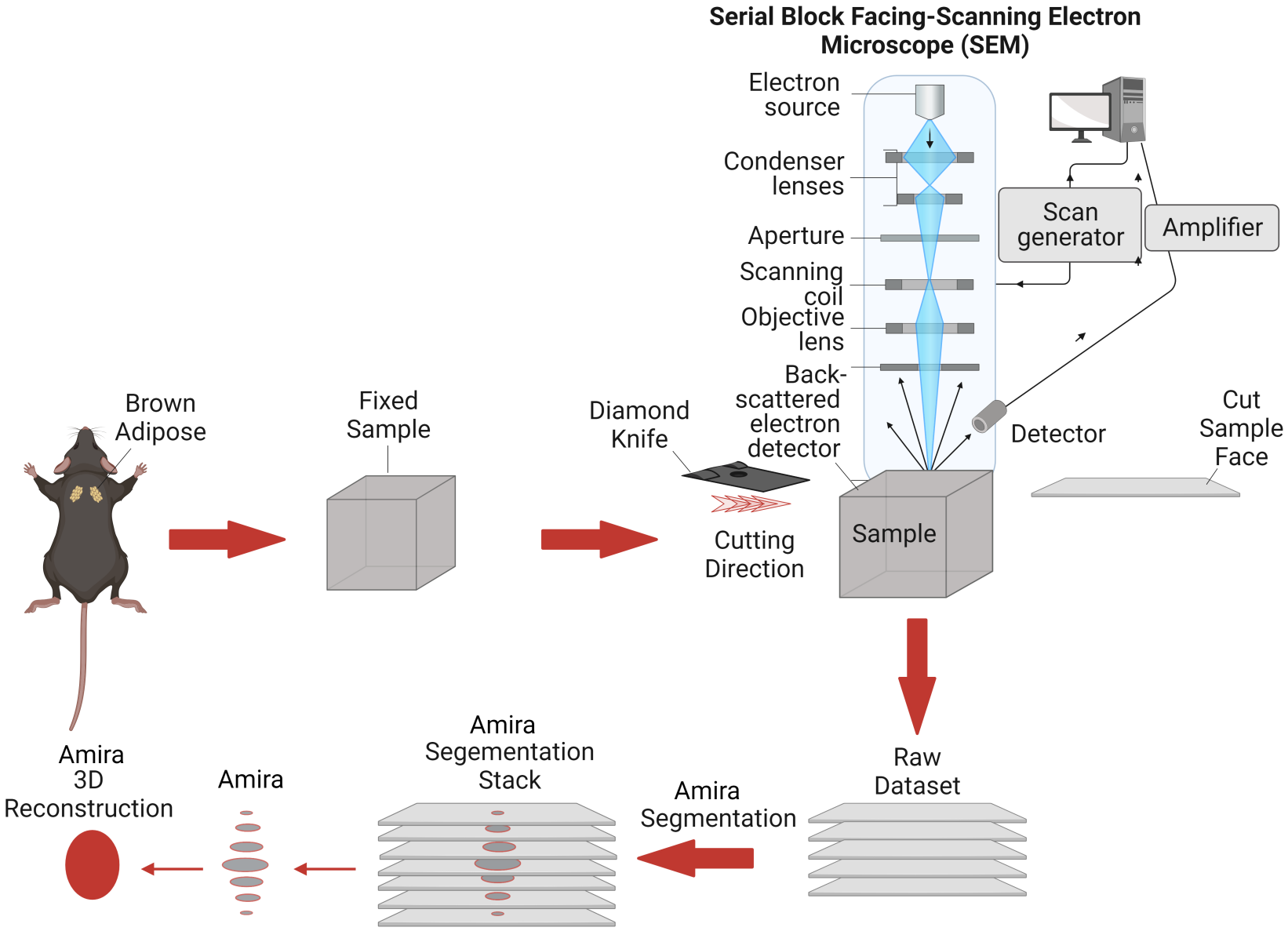

# Figure 1

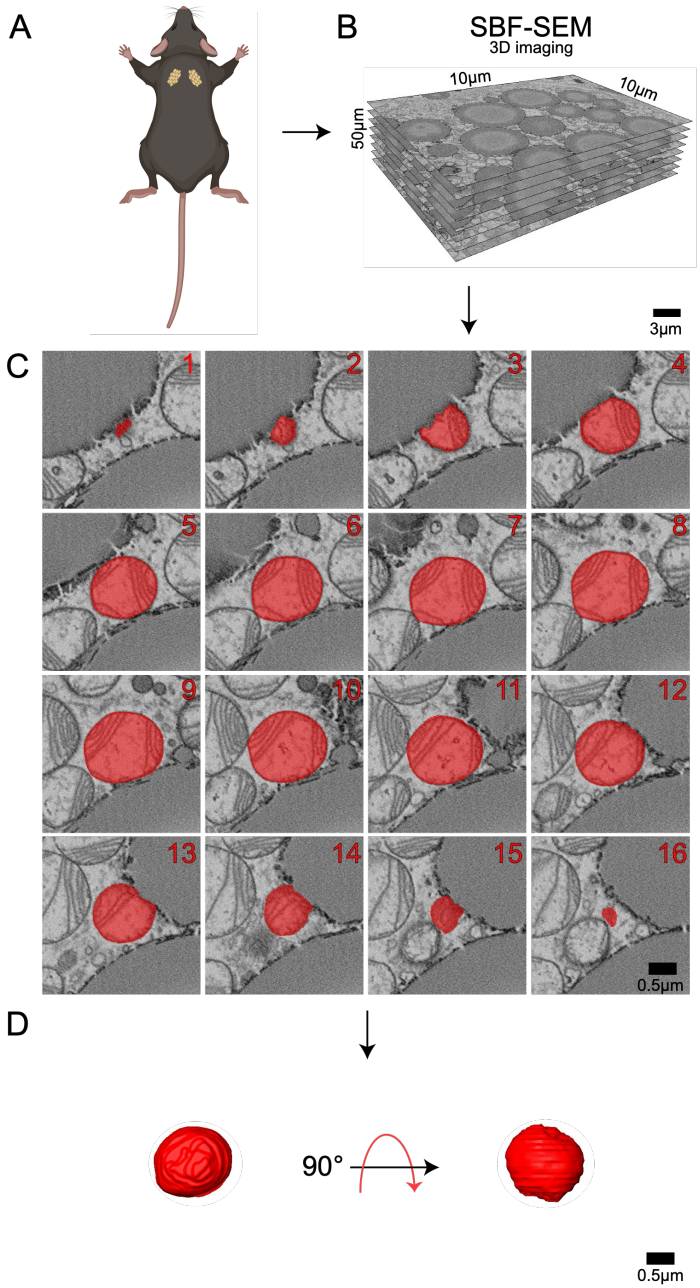
A
B
SBF-SEM
3D imaging
10µm
10µm
50µm
3µm
C
1
2
3
4
5
6
7
8
9
10
11
12
13
14
15
16
0.5µm
D
90°
0.5µm

# Figure 2

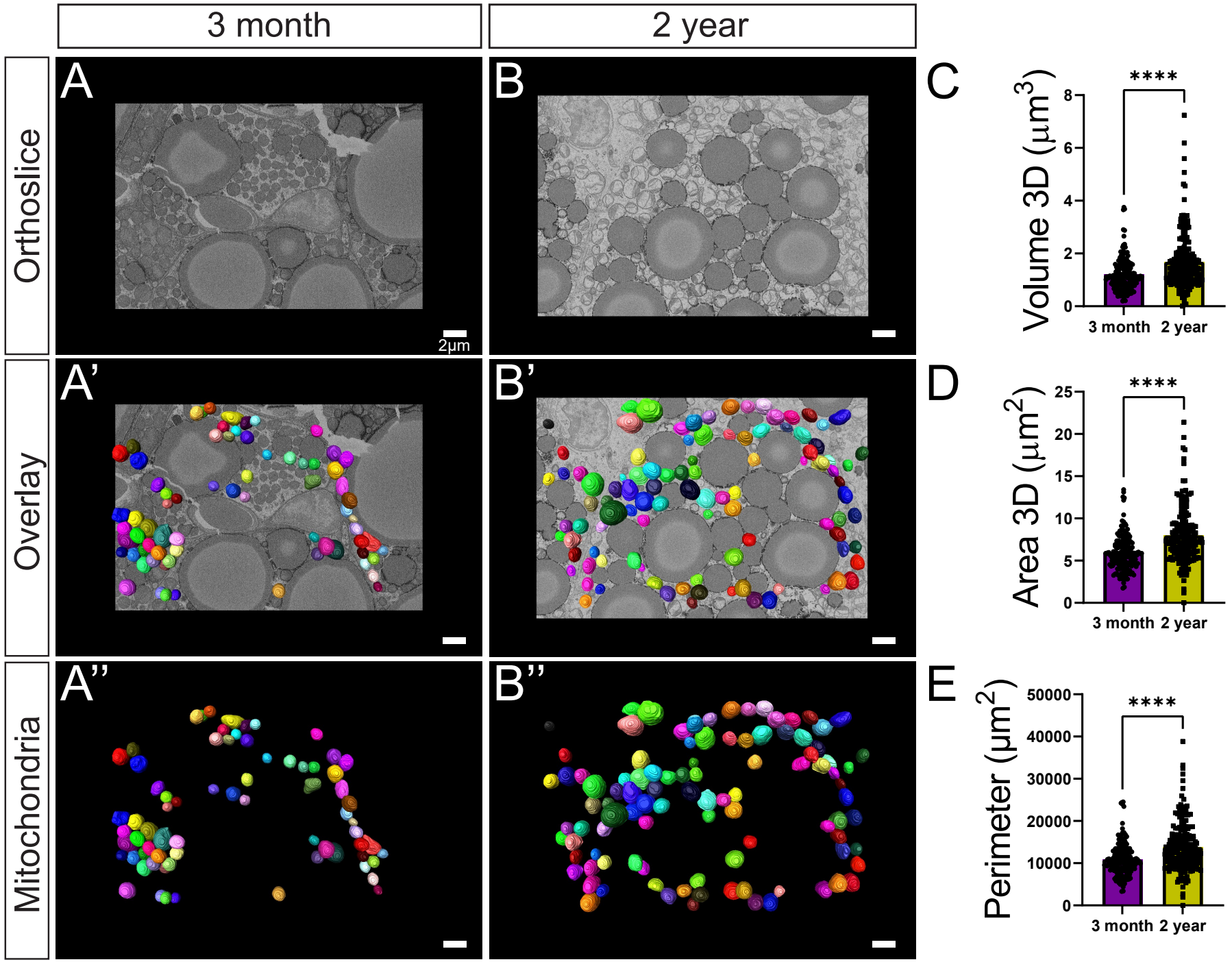
3 month
2 year
Orthoslice
Overlay
Mitochondria
A
B
A'
B'
A''
B''
2µm
C
D
E
Volume 3D (µm3)
Area 3D (µm2)
Perimeter (µm2)
****
3 month
2 year

# Figure 3

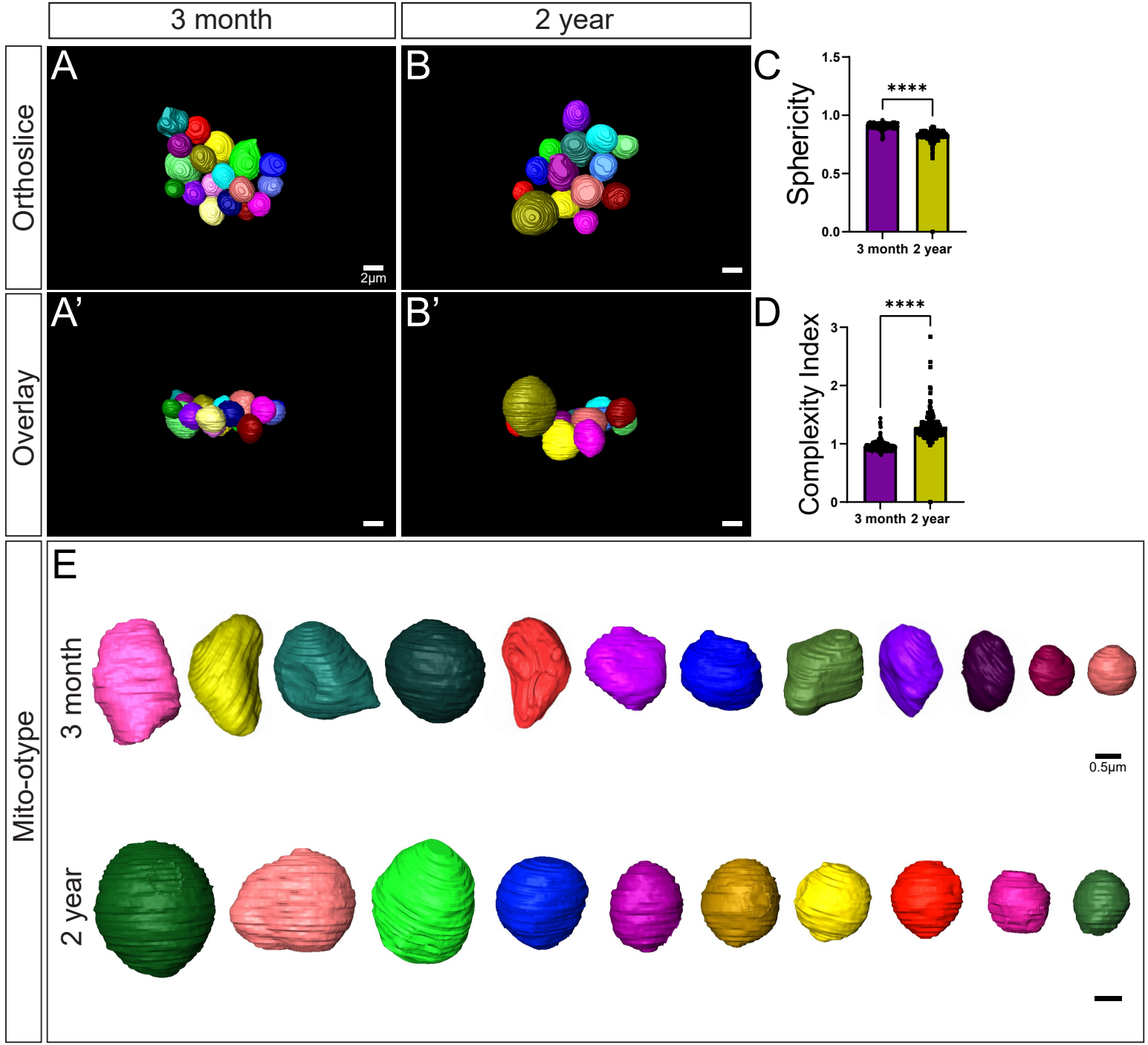
3 month
2 year
Orthoslice
Overlay
Mito-otype
A
B
C
A'
B'
D
E
2μm
Sphericity
1.5
1.0
0.5
0.0
****
3 month
2 year
Complexity Index
3
2
1
0
****
3 month
2 year
3 month
2 year
0.5μm

# Figure 4

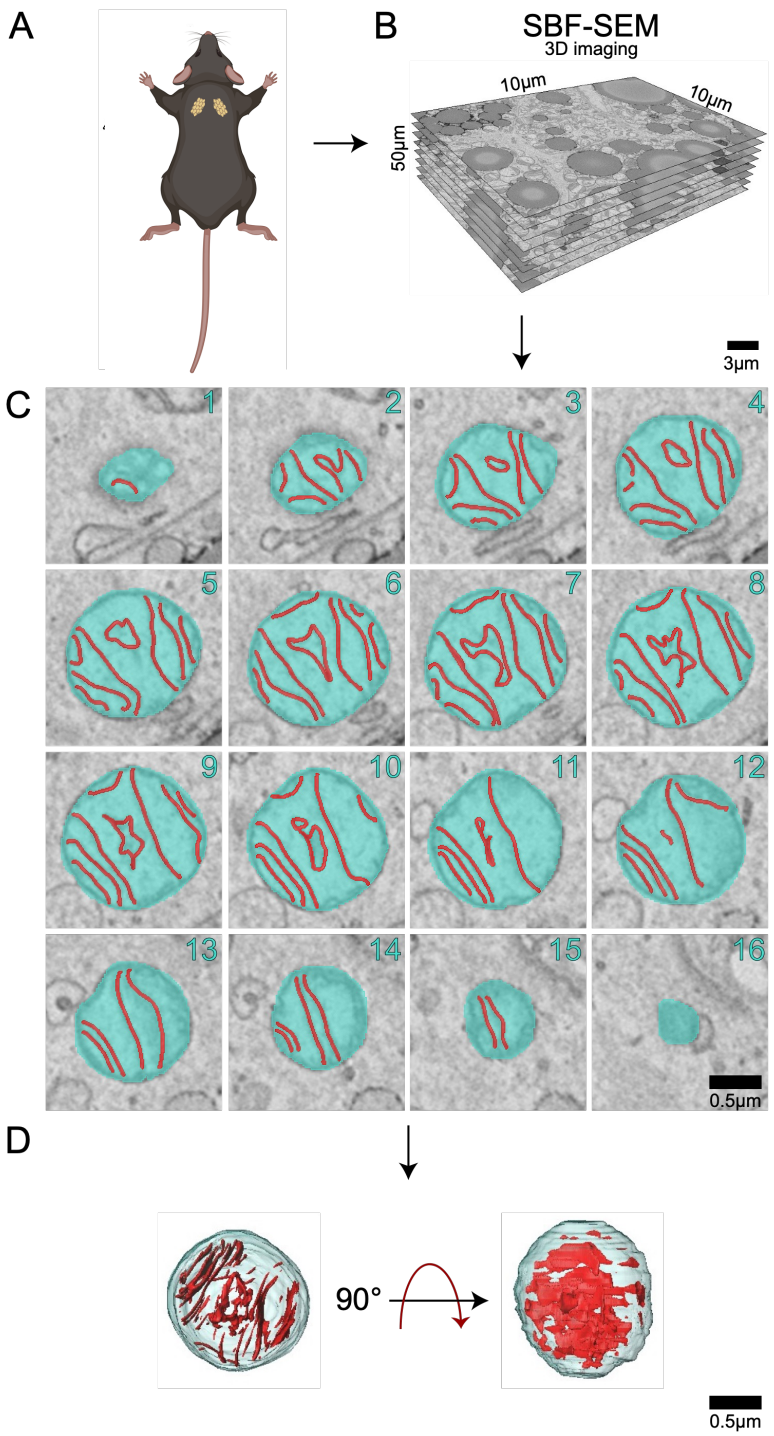
A
B
SBF-SEM
3D imaging
10µm
10µm
50µm
3µm
C
1
2
3
4
5
6
7
8
9
10
11
12
13
14
15
16
0.5µm
D
90°
0.5µm

# Figure 5

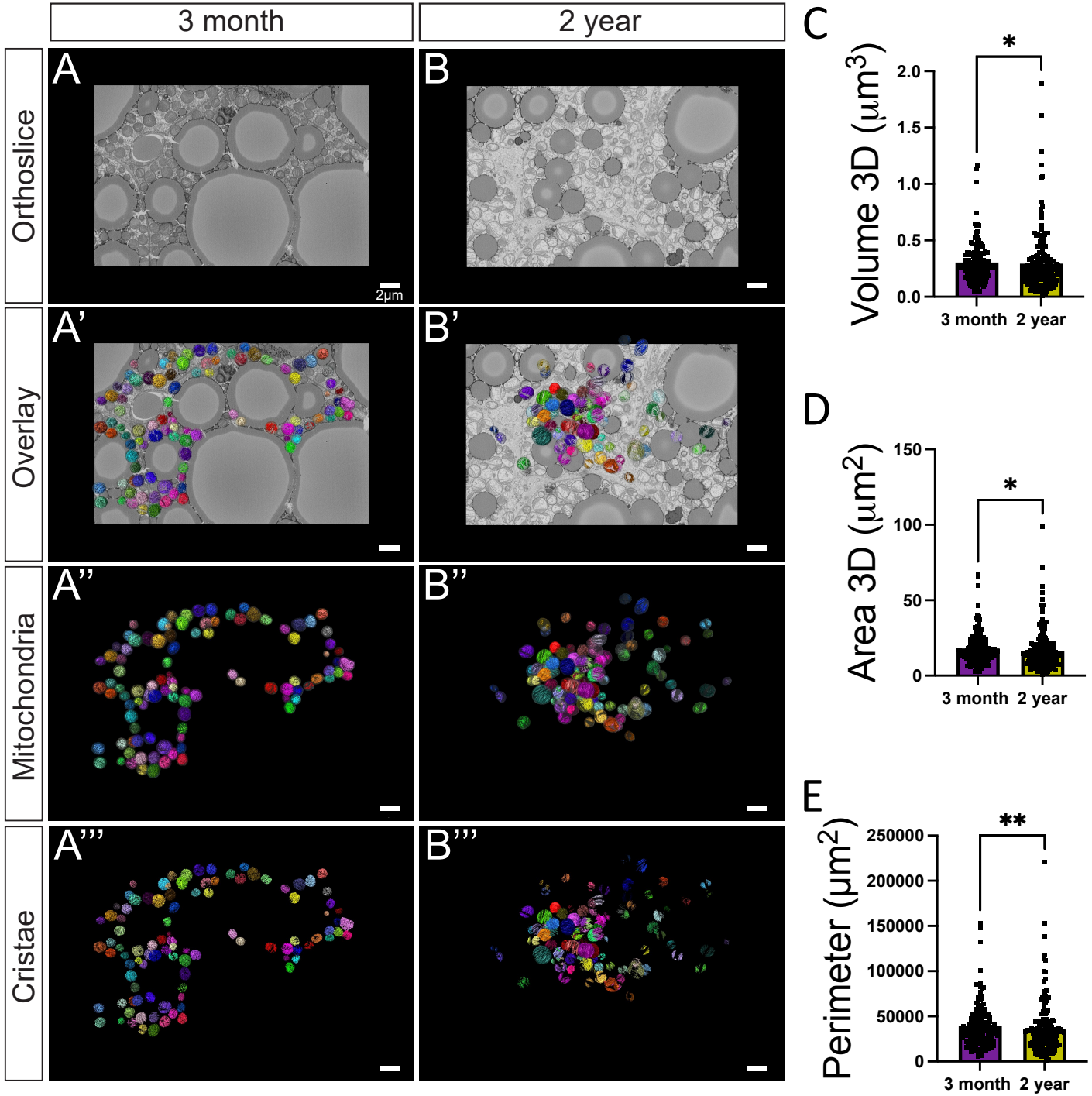
3 month
2 year
Orthoslice
Overlay
Mitochondria
Cristae
A
B
A'
B'
A''
B''
A'''
B'''
2µm
C
Volume 3D (µm³)
2.0
1.5
1.0
0.5
0.0
*
3 month
2 year
D
Area 3D (µm²)
150
100
50
0
*
3 month
2 year
E
Perimeter (µm²)
250000
200000
150000
100000
50000
0
**
3 month
2 year

# Figure 6

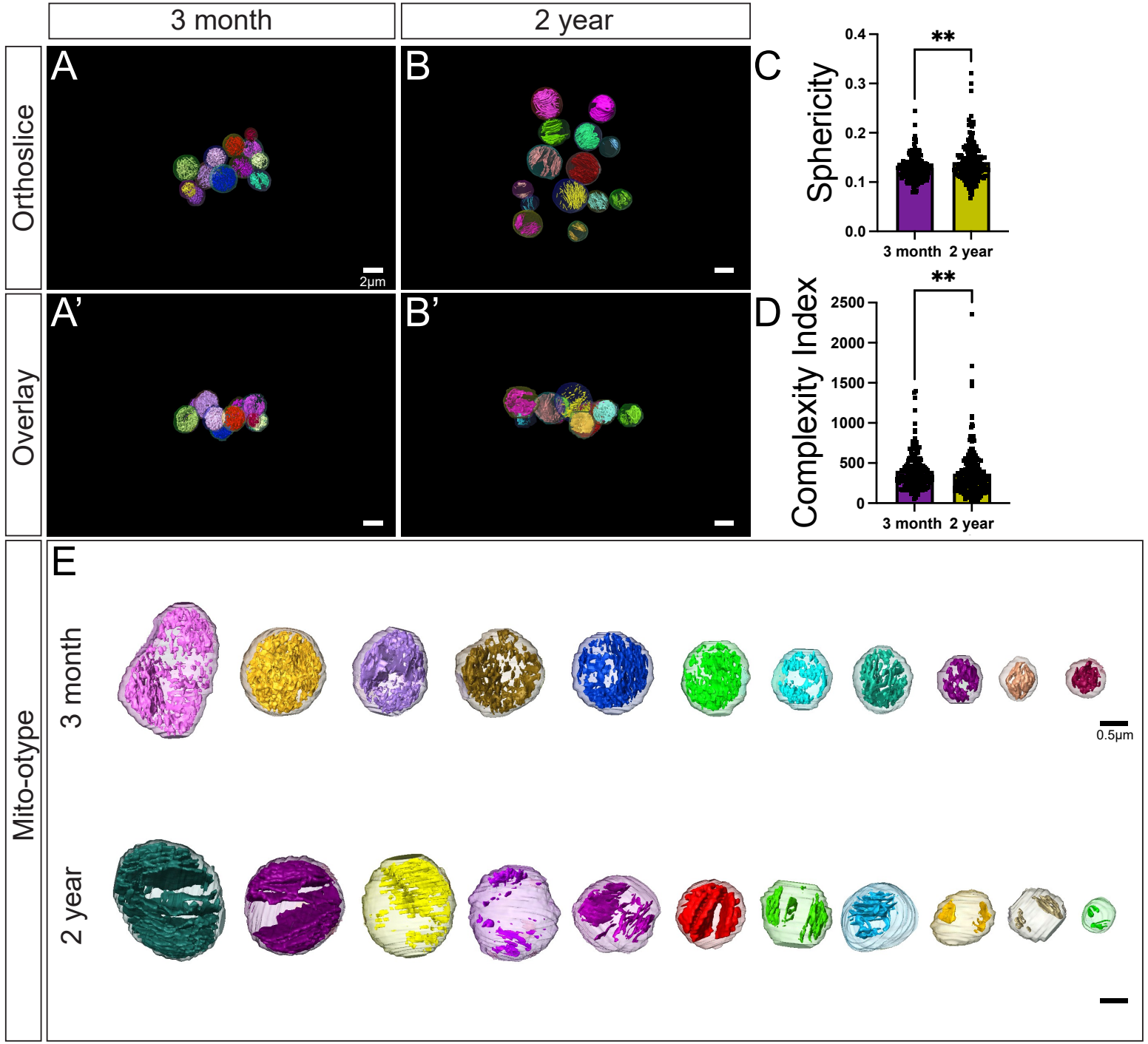
3 month
2 year
Orthoslice
Overlay
Mito-otype
A
B
C
A'
B'
D
E
2μm
Sphericity
0.4
0.3
0.2
0.1
0.0
**
3 month
2 year
Complexity Index
2500
2000
1500
1000
500
0
**
3 month
2 year
3 month
2 year
0.5μm